NASA CONTRACTOR REPORT 166387

NASA-CR-166387
19820023424

Singularity Embedding Method in Potential Flow Calculations

Wen-Huei Jou
Hung Huynh

NASA Purchase Order A-77471B
June 1982

NASA

NASA CONTRACTOR REPORT 166387

Singularity Embedding Method in Potential Flow Calculations

Wen-Huei Jou
Hung Huynh
Flow Research Company
Kent, Washington

Prepared for Ames Research Center
under NASA Purchase Order A-77471B

National Aeronautics and
Space Administration

Ames Research Center
Moffett Field, California 94035

Flow Research Report No. 216

Singularity Embedding Method in Potential Flow Calculations *

by

Wen-Huei Jou
Hung Huynh

January 1982

Flow Research Company
A Division of Flow Industries, Inc.
21414-68th Avenue South
Kent, Washington 98031
(206)872-8500

*This work was supported by the Applied Computational Aerodynamics Branch, NASA-Ames Research Center, under Office of Naval Research Contract No. N00014-80-C-0453.

Abstract

The so-called H-type mesh is used in a finite-element (or finite-volume) calculation of the potential flow past an airfoil. Due to coordinate singularity at the leading edge, a special singular trial function is used for the elements neighboring the leading edge. The results using the special singular elements are compared to those using the regular elements. It is found that the unreasonable pressure distribution obtained by the latter is removed by the embedding of the singular element. Suggestions to extend the present method to transonic cases are given.

Table of Contents

List of Figures

1. Introduction

In finite-volume calculations of the potential flow around an airfoil (Jameson and Caughey, 1977), the physical space is mapped to a computational space in which the airfoil is mapped to a horizontal or vertical line segment and a rectangular mesh is created. The velocity potential in the rectangular element is then represented by a bilinear function of the computational variable for a two-dimensional calculation. This process assumes that the transformation from physical space to computational space is regular everywhere. Because of this assumption, the type of mesh one can use is restricted. For an airfoil calculation, a C-type or O-type mesh which wraps around the leading edge is commonly used, while the H-type mesh (see Figure 1) which has a transformation singularity at the leading edge is usually considered not suitable for calculation. However, the latter has some advantages in the geometrical description of a complex three-dimensional configuration. An obvious example is the canard-wing combination. In order to place the shed vortex on the prescribed surface, the wakes coming off the canard and the wing must be on mesh lines. It is impossible for a C-type or an O-type mesh to fulfill this requirement. For an H-type mesh, this requirement can be satisfied fairly easily. Since we know that the difficulty with an H-type mesh stems from the singularity of the geometrical transformation, there must be a way to "undo" this singularity.

In this report, we represent the potential and the transformation function near the transformation singularity by a trial function which reflects the local singular behavior in the computational space. This singular behavior cannot be represented by the conventional bilinear trial function and has been the heart of the problem in using the H-type mesh. Since the problem we are dealing with is common in all Mach number ranges, we have chosen to work with incompressible flow. The method developed here can, however, be extended to the transonic case.

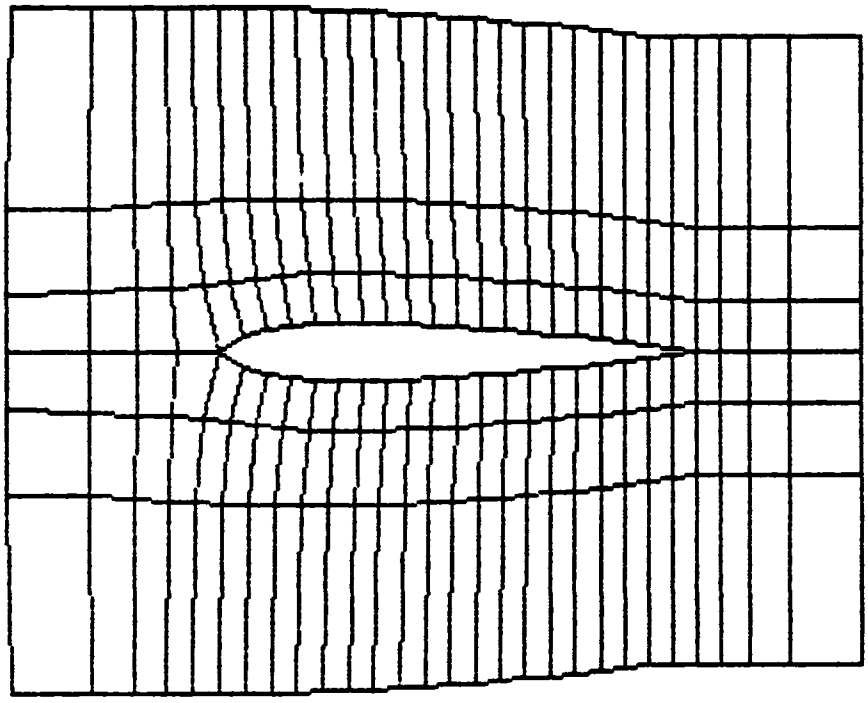

Figure 1. H-type Mesh

2. Finite-Element Formulation

Consider the two-dimensional Laplace equation

$$-\phi_{xx} - \phi_{yy} = 0 \tag{1}$$

with the far field Dirichlet boundary condition at infinity and the Neumann boundary condition on the airfoil. Variational principle for this problem states that solving Equation (1) together with the boundary conditions is equivalent to minimizing the quadratic functional

$$I(f) = \int \left[\left(\frac{\partial f}{\partial x}\right)^2 + \left(\frac{\partial f}{\partial y}\right)^2 \right] dx\, dy \tag{2}$$

for appropriate functions f which are square integrable [i.e., the right-hand side of Equation (2) is finite] together with their first-order derivatives (Strang and Fix, 1973).

In the following finite-element formulation, we first generate a mesh of quadrilaterals in the physical space. For each cell ω, the mesh is then mapped to a unit square Ω in computational space by the transformation $X = X(x, y)$ and $Y = Y(x, y)$. It is more convenient to estimate $I(f)$ in computational space. Therefore, we shall need the following formula for the change of variable. Let f be any function on ω and F be the corresponding function on Ω, i.e., $F(X, Y) = f(x, y)$. Applying the chain rule and the change of variable formula to Equation (2) we have

$$I(f) = \int_{\Omega} \left[(F_X y_Y - F_Y y_X)^2 + (F_Y x_X - F_X x_Y)^2 \right] h^{-1}\, dX\, dY \quad , \tag{3}$$

where h is the Jacobian

$$h = x_X y_Y - x_Y y_X \quad . \tag{4}$$

The variational problem is now completely handled in the transformed space. The variation of F within the computational element Ω is represented by some trial function having four corner values (α_1, α_2, α_3, α_4) as parameters. The elements are divided into two groups: regular elements in which the function F can be locally approximated by a bilinear function and special

elements in which F as well as the mapping (x, y) → (X, Y) are singular and special functional forms must be chosen.

In the following, we shall deal with the interior elements first. Treatment of the boundary elements is given in Section 3.

Regular Elements

A schematic representation of the transformation between the physical space and the computational space is shown in the following figure.

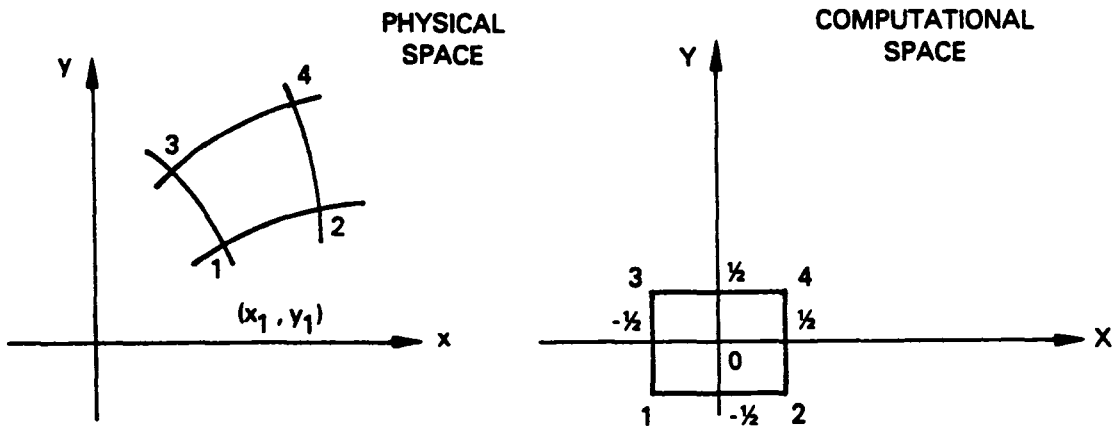

Figure 2. Transformation Between Physical and Computational Space

The local relationship between physical and computational coordinates is

$$x = \left(\tfrac{1}{2} - X\right)\left(\tfrac{1}{2} - Y\right) x_1 + \left(\tfrac{1}{2} + X\right)\left(\tfrac{1}{2} - Y\right) x_2 + \left(\tfrac{1}{2} - X\right)\left(\tfrac{1}{2} + Y\right) x_3 + \left(\tfrac{1}{2} + X\right)\left(\tfrac{1}{2} + Y\right) x_4 \quad . \tag{5}$$

A similar expression holds for y.

In general, a bilinear function on the square cell (1, 2, 3, 4) with corner values $(\alpha_1, \alpha_2, \alpha_3, \alpha_4)$ has the form

$$F = \left(\tfrac{1}{2} - X\right)\left(\tfrac{1}{2} - Y\right) \alpha_1 + \left(\tfrac{1}{2} + X\right)\left(\tfrac{1}{2} - Y\right) \alpha_2 + \left(\tfrac{1}{2} - X\right)\left(\tfrac{1}{2} + Y\right) \alpha_3 + \left(\tfrac{1}{2} + X\right)\left(\tfrac{1}{2} + Y\right) \alpha_4 \quad . \tag{6}$$

Using Equation (5), the expression for h in Equation (4) can be written as a linear function in X and Y:

$$h = h_0 + h_X X + h_Y Y \tag{7}$$

where

$$h_0 = \frac{1}{2}(x_2 - x_1 + x_4 - x_3)(y_3 - y_1 + y_4 - y_2) - \frac{1}{2}(x_3 - x_1 + x_4 - x_2)(y_2 - y_1 + y_4 - y_3) \tag{8}$$

and

$$h_X = (x_2 - x_1)(y_4 - y_3) - (x_4 - x_3)(y_2 - y_1)$$
$$h_Y = (x_4 - x_2)(y_3 - y_1) - (x_3 - x_1)(y_4 - y_2) \quad . \tag{9}$$

The finite-volume scheme of Jameson and Caughey (1977) approximates h by its value at the center of the cell. Here, we try to extend the accuracy one order higher by approximating h^{-1} in Equation (3) with a linear function. This can be done easily by binomial expansion.

Using Equations (5), (6) and (7), the integral of Equation (3) in a regular element can be obtained as a quadratic functional of the corner potential values α_1, α_2, α_3 and α_4. By summing the integrals from all the elements, I(f) is approximated by a quadratic expression of the potentials at the mesh points (F_{ij}). Minimizing I is equivalent to solving for a system of linear equations:

$$\frac{\partial I}{\partial F_{ij}} = 0 \quad . \tag{10}$$

The coefficients of this set of linear equations form the so-called stiffness matrix. The general expression of this stiffness matrix is quite cumbersome and will not be given here. For an identity transformation, the weight in the stiffness matrix is distributed as shown in the following figure. It is the sum of a five-point formula and a rotated (45°) five-point formula.

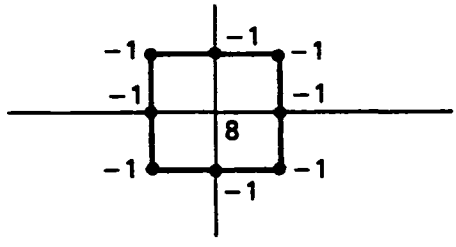

Figure 3. Stencil of Stiffness Matrix

Special Elements

The transformation from physical to computational space is set up to be analytic in the four cells at the leading edge except at the leading edge itself, and it transforms these cells to four squares of unit area.

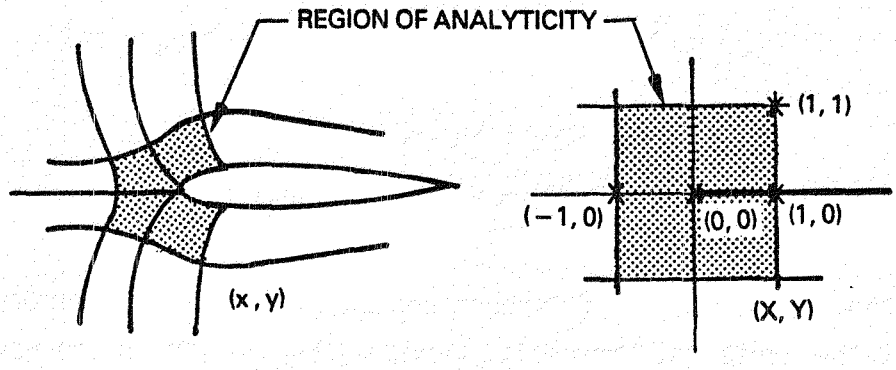

Figure 4. Transformation Near Singularity

It is well known that a function which is regular in the physical space behaves as $r^{1/2}$ in the transformed space. Thus, rather than using a bilinear function and packing the mesh densely at the leading edge to approximate the singular solution, we use four special elements.

On the triangle (1, 2, 4) shown in Figure 5, consider the function

$$F = \alpha_1 + (\alpha_2 - \alpha_1)X^{1/2} + (\alpha_4 - \alpha_2)YX^{-1/2} \qquad (11)$$

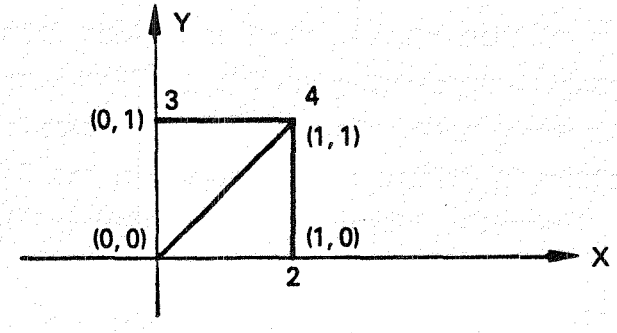

Figure 5. Special Element

Clearly such a function attains the values α_1, α_2 and α_4 at corners 1, 2 and 4; furthermore, it is linear on the edge (2, 4) which would assure continuity between special and regular elements. Along edge (1, 4), two such

functions from neighboring triangles are identical so that continuity between special elements is preserved. Heuristically, $X^{1/2}$ should pick up $r^{1/2}$ behavior and the variation of corner values α_2 and α_4 should reflect the angular variations. A similar formula with the reverse roles of X and Y can be applied to the triangle (1, 3, 4).

Let f be the function in physical space corresponding to F, which is of the form of Equation (11). We now evaluate I(f). By analyticity, we have the Cauchy-Riemann equations:

$$x_X = y_Y \ , \ x_Y = -y_X \tag{12}$$

Substituting these equations into the Jacobian expression given as Equation (4), Equation (3) can be written as

$$I(f) = \int \left[\left(\frac{\partial F}{\partial X}\right)^2 + \left(\frac{\partial F}{\partial Y}\right)^2 \right] dX \, dY \tag{13}$$

Note that Equation (13) is similar to Equation (2) except that we have F in the integral on the right-hand side instead of f.

The four special elements are broken into eight triangles, in each of which the trial function is assumed to be of the form of Equation (8). A calculation of the $\partial I/\partial\alpha$ terms using Equation (13) for I gives the following expression for the contribution to the stiffness matrix from the element shown in Figure 5:

$$\begin{aligned}
\frac{\partial I}{\partial \alpha_1} &: \quad \alpha_1 - \frac{3}{4}\alpha_2 - \frac{3}{4}\alpha_3 + \frac{1}{2}\alpha_4 \\
\frac{\partial I}{\partial \alpha_2} &: -\frac{9}{12}\alpha_1 + \frac{38}{12}\alpha_2 - \frac{29}{12}\alpha_4 \\
\frac{\partial I}{\partial \alpha_3} &: -\frac{9}{12}\alpha_1 + \frac{38}{12}\alpha_3 - \frac{29}{12}\alpha_4 \\
\frac{\partial I}{\partial \alpha_4} &: \quad \frac{1}{2}\alpha_1 - \frac{29}{12}\alpha_2 - \frac{29}{12}\alpha_3 + \frac{52}{12}\alpha_4
\end{aligned} \tag{14}$$

We can take advantage of the permutational symmetry of the special elements to obtain the contribution to the stiffness matrix by the other three.

The element stiffness matrix for each cell is computed and the results are assembled to give the global stiffness matrix K.

3. Boundary Conditions

Let Φ be a potential which satisfies Equation (1) together with the boundary conditions. Let $\Phi_\infty = x \cos \alpha + y \sin \alpha$ be the undisturbed potential with flow angle α. Instead of solving for Φ, it is more convenient to solve for the reduced potential $G = \Phi - \Phi_\infty$. The boundary conditions on Φ must be transformed to those on the reduced potential G.

Far Field Boundary Condition

The far field boundary condition is given iteratively as the potential vortex field generated by the lift. Consider the far field boundary cell (1, 2, 3, 4) shown in Figure 6.

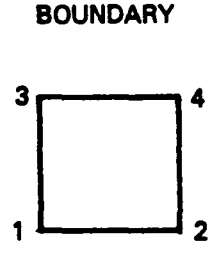

Figure 6. Far Field Boundary Cell

Let edge (3, 4) be part of the boundary. In solving for the solution α_i values, which are corner values of G, α_3 and α_4 are given by the potential vortex obtained from the previous iteration. Hence, one assembles the stiffness matrix for this boundary cell in the same way as for an interior cell. In computing the solution, terms involving α_3 and α_4 are known quantities and are moved to the right-hand side of the equation.

Neumann Boundary Condition

The Neumann boundary condition on the airfoil for Φ is $\partial_{\vec{n}} \Phi = 0$, where $\vec{n}$ is the outward normal unit vector to the airfoil (See Figure 7). While the boundary condition for Φ is the so-called natural boundary condition in the variational method, that on G requires some modification. The corresponding boundary condition for G is

$$\partial_{\vec{n}} G = - \partial_{\vec{n}} \Phi_\infty \quad . \tag{15}$$

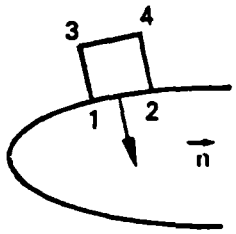

Figure 7. Cell With Neumann Boundary Condition

Consider now a cell with the Neumann boundary condition on edge (1, 2). Then, Equation (15) together with the expression for Φ_∞ takes the form

$$\partial_{\vec{n}} G = - n_1 \cos\alpha - n_2 \sin\alpha \tag{16}$$

where n_1 and n_2 are x- and y-components of $\vec{n}$ [the outward normal of the line segment (1, 2)].

For a cell with the Neumann boundary condition as in Figure 7, we define

$$I(g) = \int_{\text{cell}} \left(g_x^2 + g_y^2\right) dx\, dy + 2 \oint (n_1 \cos\alpha + n_2 \sin\alpha) g \, d\sigma \tag{17}$$

where $\oint d\sigma$ is the integration on the line segment (1, 2). We next reproduce the well-known proof that if G is a function which minimizes I(g), then G satisfies Equation (16) (Strang and Fix, 1973). Let ε be a real number, then

$$\begin{aligned} I(G + \varepsilon H) &= \int \left(G_x^2 + G_y^2\right) dx\, dy + \varepsilon^2 \int \left(H_x^2 + H_y^2\right) dx\, dy \\ &\quad + 2\varepsilon \int (G_x H_x + G_y H_y)\, dx\, dy + 2 \oint (n_1 \cos\alpha + n_2 \sin\alpha)\, (G + \varepsilon H)\, d\sigma \\ &= I(G) + 2\varepsilon \int (G_x H_x + G_y H_y)\, dx\, dy + 2\varepsilon \oint (n_1 \cos\alpha + n_2 \sin\alpha) H \, d\sigma \\ &\quad + \varepsilon^2 \int \left(H_x^2 + H_y^2\right) dx\, dy \,. \end{aligned} \tag{18}$$

Since G minimizes I(g), the ε term in Equation (18) must vanish, i.e.,

$$\int (G_x H_x + G_y H_y)\, dx\, dy + \oint (n_1 \cos\alpha + n_2 \sin\alpha) H \, d\sigma = 0 \tag{19}$$

for any function H such that $I(H) < \infty$. Integrating by parts, we have

$$-\int (G_{xx} + G_{yy}) H \, dx \, dy + \oint \left[\left(\partial_{\vec{n}} G \right) + \left(n_1 \cos \alpha + n_2 \sin \alpha \right) \right] H \, d\sigma = 0. \qquad (20)$$

Since H is arbitrary except for the constraint that $I(H) < \infty$, each integral in the above expression must vanish independently. The vanishing of the second implies Equation (16).

Thus, cells with Neumann boundary conditions differ from interior cells only by the second term on the right-hand side of Equation (17). Using the linear expression for G on the line segment (1, 2), this term can be estimated as follows:

$$\begin{aligned} 2 \oint & \left(n_1 \cos \alpha + n_2 \sin \alpha \right) G \, d\sigma \\ &= 2L \int_{-1/2}^{1/2} \left(n_1 \cos \alpha + n_2 \sin \alpha \right) \left[\left(\tfrac{1}{2} - X \right) \alpha_1 + \left(\tfrac{1}{2} + X \right) \alpha_2 \right] dX \\ &= L \left(n_1 \cos \alpha + n_2 \sin \alpha \right) \left(\alpha_1 + \alpha_2 \right) \end{aligned} \qquad (21)$$

where the first equality comes from Equation (6), and the second equality comes from a straightforward calculation. L is the length of the line segment (1, 2).

For the two special elements with Neumann boundary conditions, we obtain results similar to Equation (21) by using a highest order approximation. On the boundary of the special element cell, the analytic mapping can be approximated by $\xi = LX^{1/2}$ as shown in Figure 8.

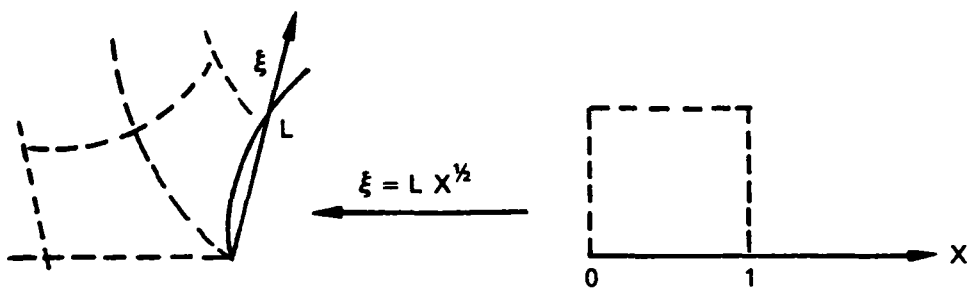

Figure 8. Local Mapping of Boundary Near Singularity

Then,
$$d\sigma = d\xi = \frac{1}{2} L X^{-1/2} \, dX \quad . \tag{22}$$

Using this together with Equation (11), we have

$$\begin{aligned} 2 \oint & (n_1 \cos\alpha + n_2 \sin\alpha) \; G \, d\sigma \\ &= L \, (n_1 \cos\alpha + n_2 \sin\alpha) \int_0^1 \left[\alpha_1 + (\alpha_2 - \alpha_1) \, X^{1/2} \right] X^{-1/2} \, dX \\ &= L \, (n_1 \cos\alpha + n_2 \sin\alpha) \; (\alpha_1 + \alpha_2) \quad . \end{aligned} \tag{23}$$

The result is identical to Equation (21).

Thus, for cells with Neumann boundary conditions, the calculation of $\partial I/\partial \alpha_1$ gives an extra term of the form

$$L \, (n_1 \cos\alpha + n_2 \sin\alpha) \; . \tag{24}$$

When solving for the α_i values, this term is known and is moved to the right-hand side of the equations.

4. Mesh Generation

The mesh is generated by the following procedure. The curvature κ of the airfoil at the leading edge is estimated by using the leading edge and two adjacent data points. A parabola of the same curvature through the leading edge is fitted in the physical space $z = x + iy$. Next, the parabola is mapped onto a semi-infinite line (0, s) in ξ space ($\xi = s + it$) by the inverse of the analytic function

$$z = i\,\xi^{1/2} + \kappa\,\xi \quad . \tag{25}$$

We can now generate a mesh of rectangles in the ξ space such that the four cells at the leading edge form four squares. The mesh in ξ space is mapped back to z space by relation (25). Finally, we use a shearing transformation to shear the parabola to the airfoil surface to obtain a body-fitted mesh system (see Figure 9).

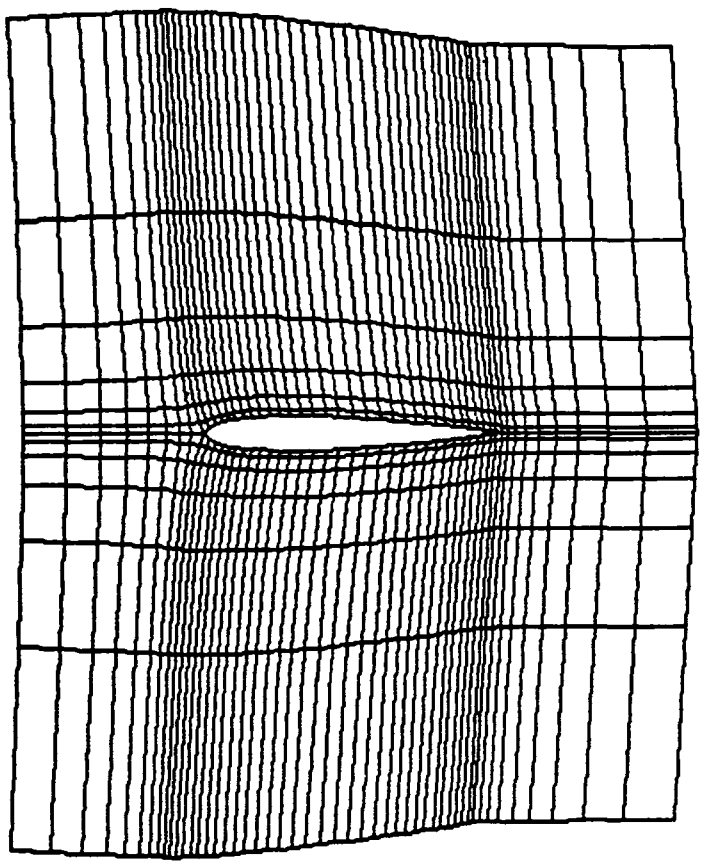

Figure 9. H-type Medium Mesh

5. Numerical Calculations and Conclusions

After gathering the stiffness matrix, the solution to the linear equation system is obtained by a horizontal line relaxation scheme. The relaxation starts at the line extending from the leading edge to the upstream infinity. Since the leading edge is a mesh singularity, the mesh line extends downstream from the leading edge along both the upper side and the lower side of the branch cut, i.e., along the upper and lower surfaces of the airfoil (Figure 10). The potential values along this entire line are updated simultaneously by a special solver. Then, the ordinary tridiagonal solver is used to relax the lines successively away from the airfoil.

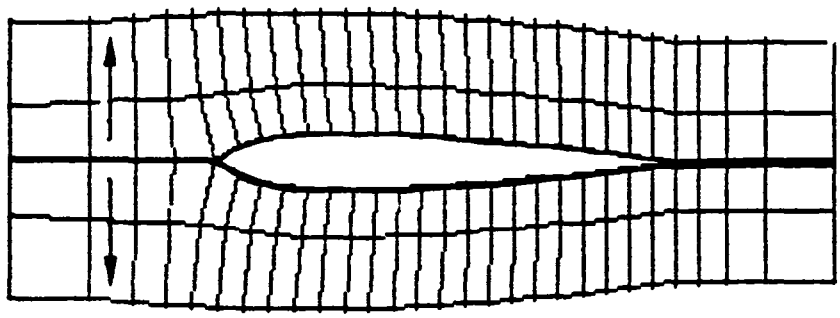

Figure 10. Line Relaxation

In order to verify the accuracy of the code, a test case for flow past a NACA 0012 airfoil is carried out with an angle of attack of 3 degrees and 300 iterations for each of the coarse, medium and fine meshes. The results (see Figures 11-16) match those of FLO 26 for a C-type mesh (finite-volume scheme, Jameson and Caughey, 1977). For the calculation using an H-type mesh with leading edge cells treated as regular elements, the pressure distribution obtained exhibits an unreasonable "kink" near the leading edge as seen in Figures 12 and 13. This "kink" seems to persist as the mesh is refined. Figures 14 and 15 show the corresponding results using special elements in four cells neighboring the leading edge. These results show that the unreasonable behavior of the pressure distribution near the leading edge is removed. For further comparison we also include the result by a panel method (Figure 16). Again, the results agree extremely well with those obtained by the finite-element method with singularity embedding.

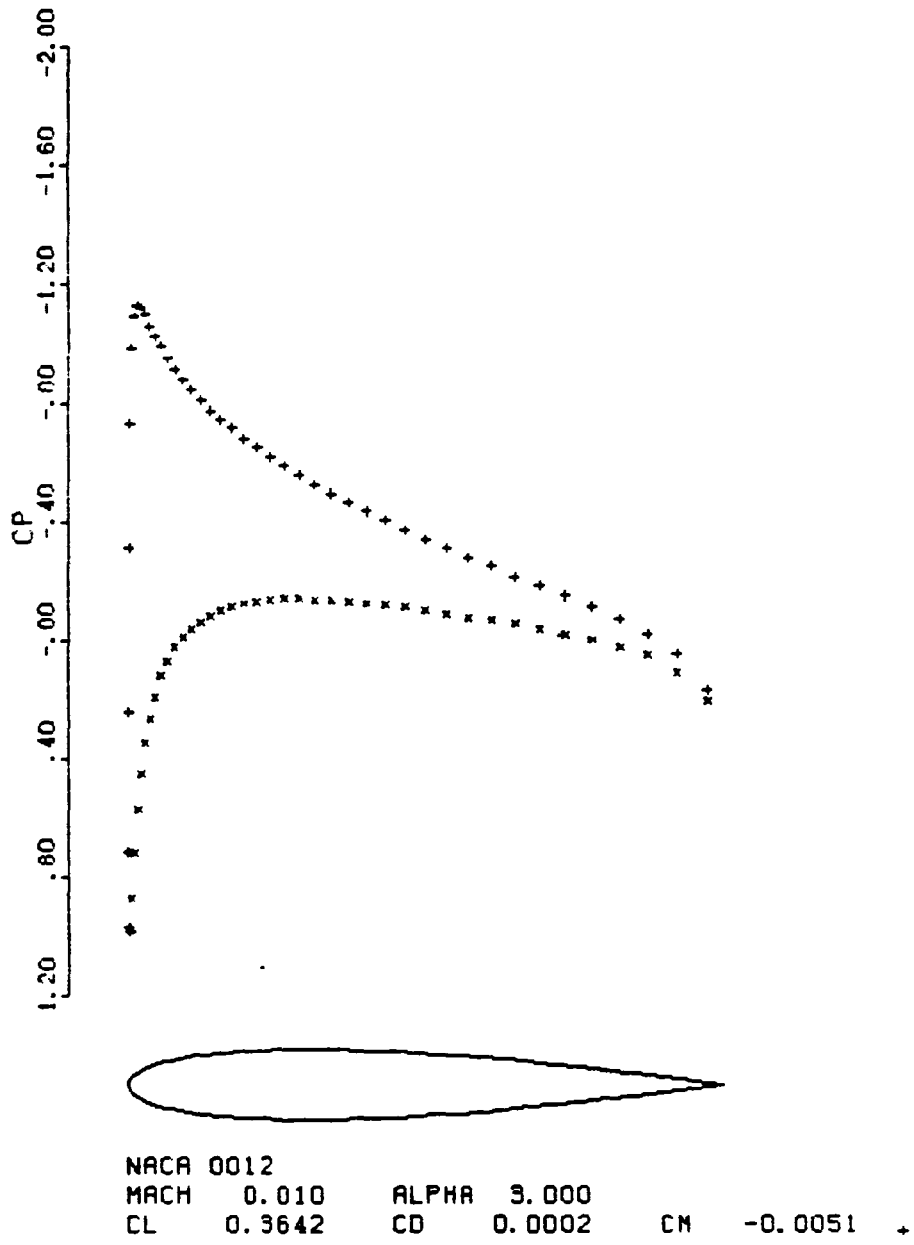

Figure 11. Finite-Volume Scheme (FLO 26)

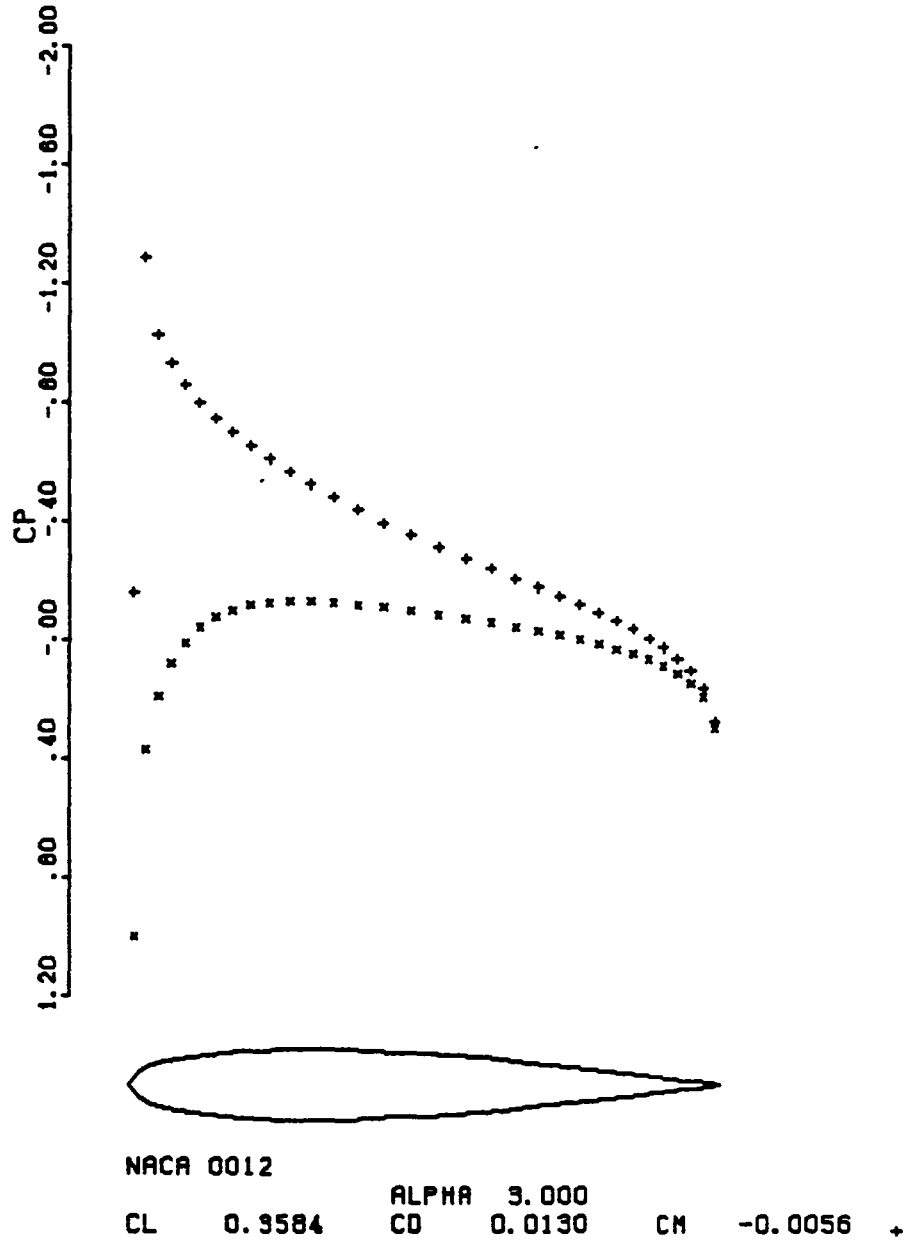

Figure 12. Regular Element Method, Medium Mesh

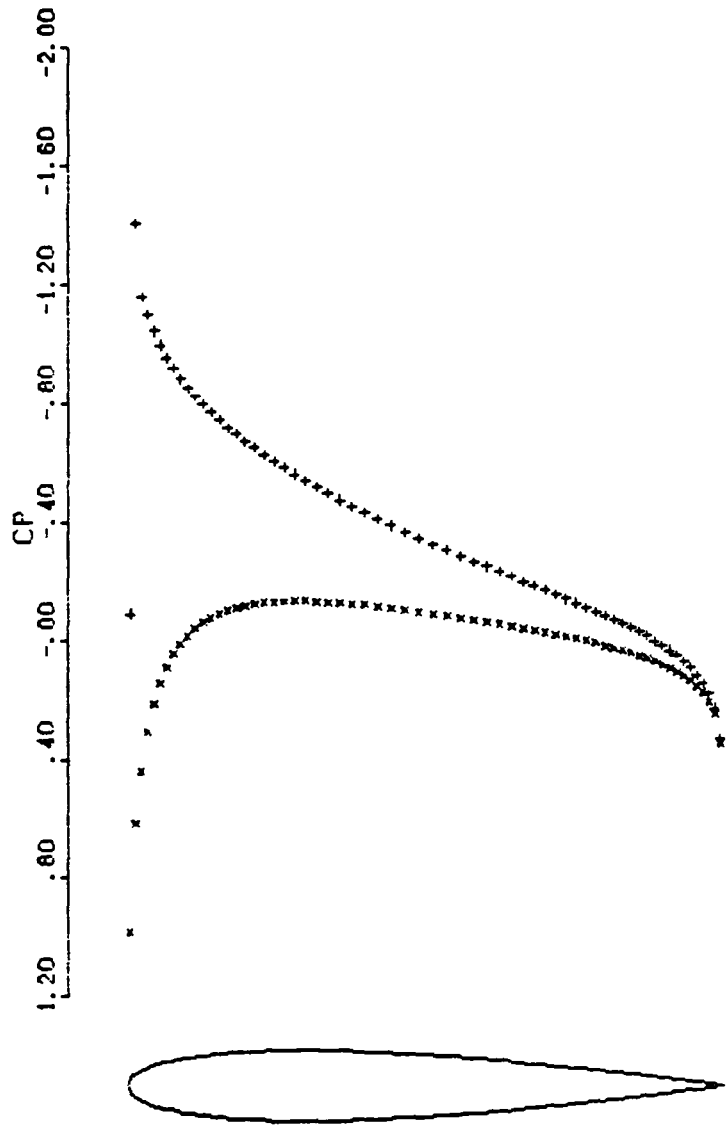

Figure 13. Regular Element Method, Fine Mesh

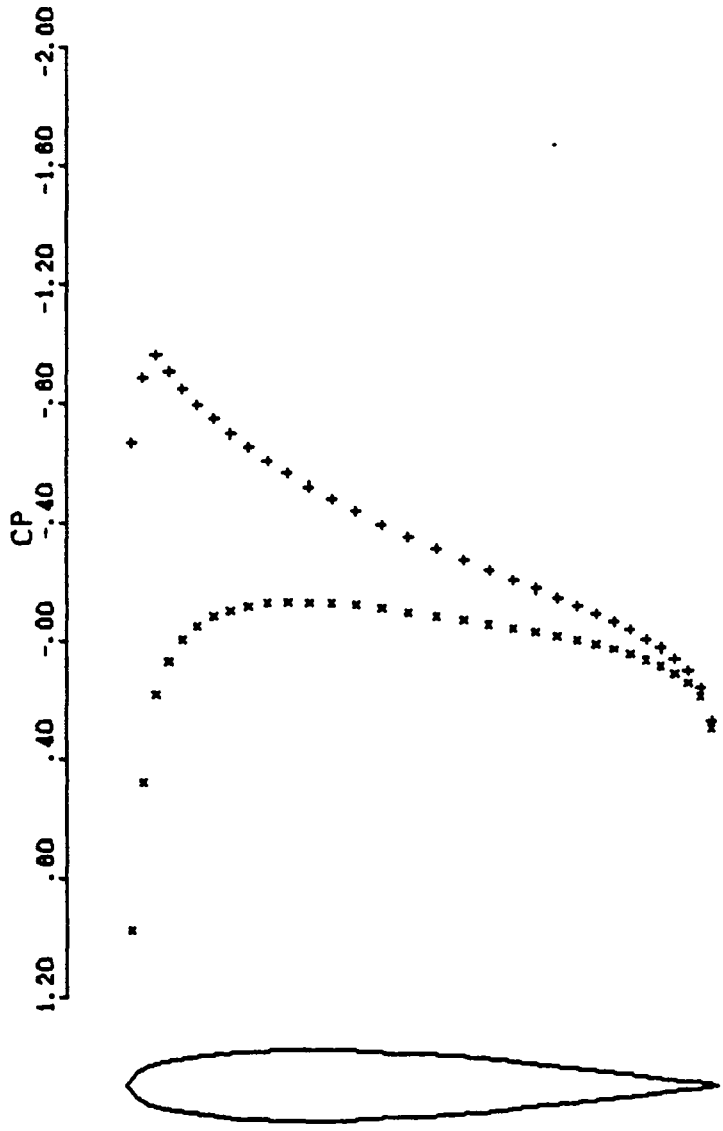

Figure 14. Special Element Method, Medium Mesh

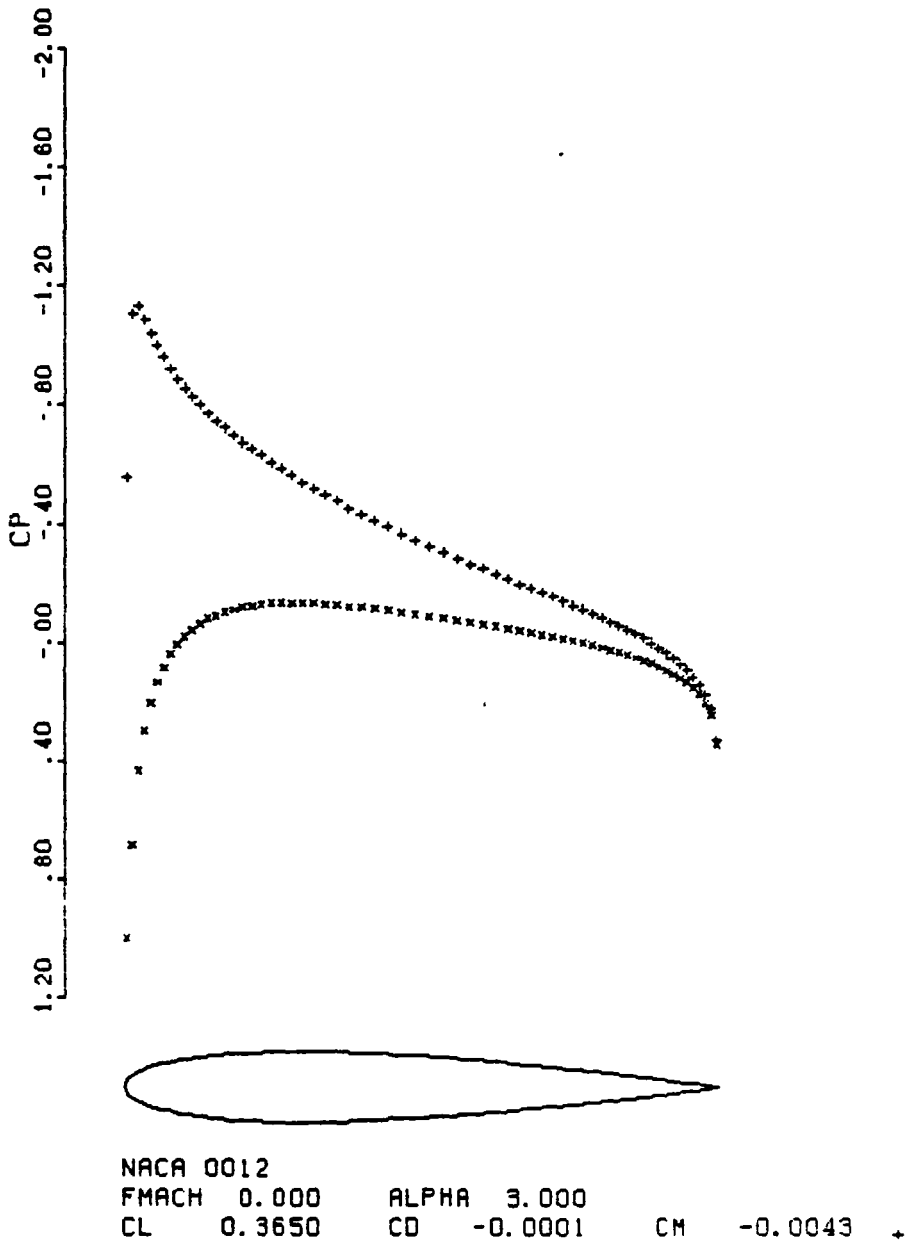

Figure 15. Special Element Method, Fine Mesh

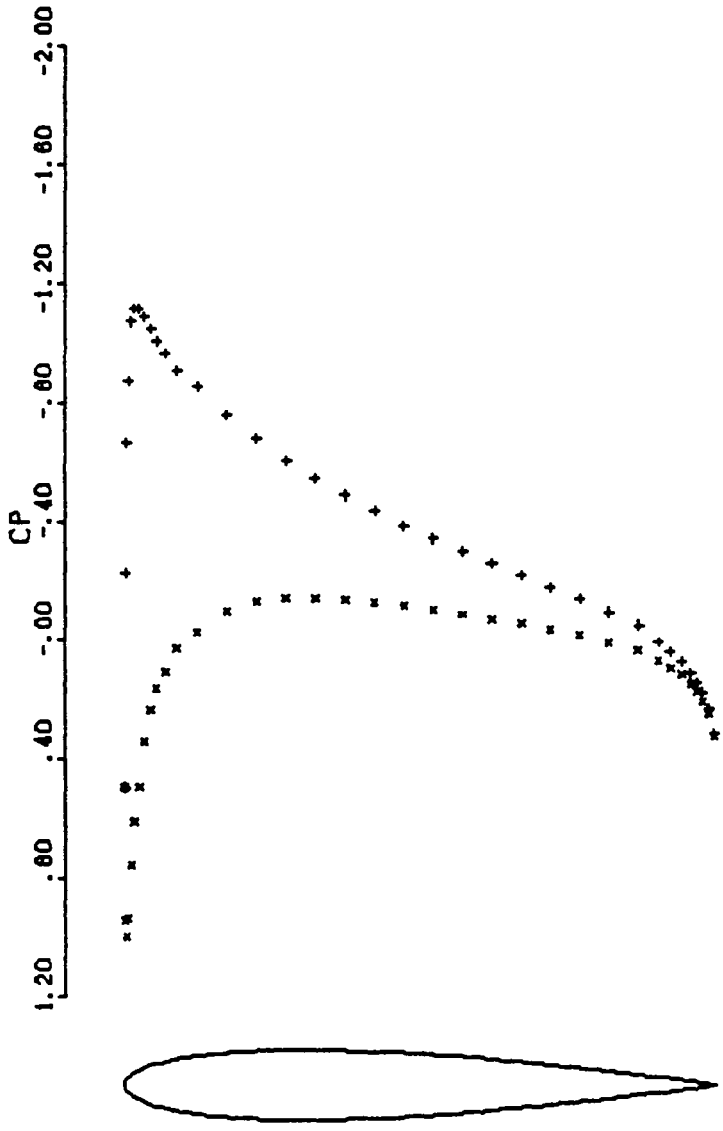

Figure 16. Panel Method

A few words can be given to the possibility of extending the present method to transonic cases. The best way seems to be adapting the artificial density concept. The conservation of mass can be written as

$$\nabla \cdot (\overline{\rho}\ \nabla\phi) = 0 \tag{26}$$

where

$$\overline{\rho} = \rho - \mu\rho_S\Delta S \tag{27}$$

is the artificial density and $\rho_S\Delta S$ is the upwind difference of the isentropic density. The nonlinear equation is solved iteratively as

$$\nabla \cdot (\overline{\rho}^{(n)}\ \nabla\phi^{(n+1)}) = 0 \tag{28}$$

where the superscript n denotes the nth approximate solution. For the (n+1)th approximation, $\overline{\rho}^{(n)}$ is a known function. The variational principle is then to minimize

$$I(\phi^{(n+1)}) = \int_\omega (\overline{\rho}\ \nabla\phi \cdot \nabla\phi)\ dx\ dy \quad . \tag{29}$$

To the degree of accuracy comparable to the existing finite-volume scheme, $\overline{\rho}$ in an element can be approximated by its value at the center of the cell. The singularity embedding method can be extended to the transonic case by multiplying the incompressible cell stiffness matrix by its cell artificial density. One also needs to modify Equation (17) for Neumann boundary conditions. The rest of the method remains unchanged. One can try to obtain a more accurate result by approximating the isentropic density by a linear function in a cell and treating the added part ($-\mu\rho_S\Delta S$) as the difference in the center value. The stiffness matrix will be more complicated, but no essential difficulty is expected.

References

Jameson, A., and Caughey, D. A. (1977) "A Finite Volume Method for Transonic Potential Flow Calculations," in Proceedings of the AIAA 3rd Computational Fluid Dynamics Conference, Albuquerque, June, pp. 35-54 (AIAA Paper No. 77-635).

Strang, G., and Fix, G. J. (1973) An Analysis of the Finite Element Method, Prentice-Hall.

WJ:589R

1 Report No.	2 Government Accession No	3 Recipient's Catalog No
NASA CR 166387		

4 Title and Subtitle	5 Report Date
Singularity Embedding Method in Potential Flow Calculations	June 1982
	6 Performing Organization Code
7 Author(s)	8 Performing Organization Report No
Wen-Huei Jou and Hung Huynh	
9 Performing Organization Name and Address	10 Work Unit No
Flow Research Company 21414-68th Ave. South Kent, Washington 98031	T-9682
	11 Contract or Grant No A-77471B
12 Sponsoring Agency Name and Address	13 Type of Report and Period Covered
National Aeronautics and Space Administration Washington, DC 20546	Contractor Report
	14 Sponsoring Agency Code

15 Supplementary Notes

Point of Contact: Dochan Kwak, NASA Ames Research Center, Moffett Field, CA 94035, (415) 965-6743, FTS 448-6743

16 Abstract

The so-called H-type mesh is used in a finite-element (or finite-volume) calculation of the potential flow past an airfoil. Due to coordinate singularity at the leading edge, a special singular trial function is used for the elements neighboring the leading edge. The results using the special singular elements are compared to those using the regular elements. It is found that the unreasonable pressure distribution obtained by the latter is removed by the embedding of the singular element. Suggestions to extend the present method to transonic cases are given.

17 Key Words (Suggested by Author(s))	18 Distribution Statement
Singularity Method H-grid Computational Aerodynamics	Unclassified - Unlimited STAR Category 02

19 Security Classif (of this report)	20 Security Classif (of this page)	21 No of Pages	22 Price*
Unclassified	Unclassified	24	

*For sale by the National Technical Information Service, Springfield Virginia 22161

End of Document